DOI 10.1007/s10778-018-0873-3
International Applied Mechanics, Vol. 54, No. 2, March, 2018

EXPERIMENTAL STUDY OF THE PLASTIC ZONE AT THE FRONT OF A MODE I CRACK

E. E. Kurchakov

The distribution of stress intensity at the front of a mode I crack in an elastic-plastic body is analyzed. From this distribution, the shape of the plastic zone is identified and its dimensions in two mutually orthogonal directions are established.

Keywords: elastic-plastic body, mode I crack, plastic zone, fracture process zone, stress intensity, hardness, experimental study

Introduction. The energy expended for fracture of elastoplastic bodies with cracks almost wholly dissipates in the plastic zone at the crack front [5]. Therefore, it is important to know the parameters of the zone and strains or stresses on its boundaries. Moreover, such parameters are needed to validate crack models. Of importance is to validate the solutions of boundary-value problems of the limiting equilibrium of elastoplastic bodies with cracks. The literature on fracture mechanics contains few data on the plastic zone due to serious obstacles that hinder experimental studies.

There are methods widely used for determining the fracture characteristics of various cracked bodies [16]. Less accurate methods are usually used to study the plastic zone, including etching methods [9, 10], photoelastic coating technique [8], replica and net methods [13, 15].

However, studying the plastic zone with the above methods requires conducting complex analysis of experimental data due to the difficulties of separating the elastic and plastic strains. Moreover, these methods can only be applied on the body's surface.

Some information on the shape and sizes of the plastic zone may be obtained from the intensity of stresses in the crack vicinity. To this end, the hardness method [6] can be used, which is based on the change in the body hardness during plastic deformation. This method assumes that the dependence of the stress intensity on hardness is invariant to the loading history. This assumption is validated by the results obtained in [7], according to which the influence of hydrostatic compression on hardness is negligible. The above assumption was also validated experimentally in [1–3], from which it follows that the difference in the data obtained does not exceed 10%.

It should be noted that the above method is not free of certain disadvantages. One of them is related to the determination of hardness attributed to the cold-hardening of the surface layer, which must be eliminated. Indentation causes local plastic deformation of the body. However, as shown in [6], the results obtained in determining the hardness are scarcely affected by this deformation, owing to which its influence can be neglected.

The purpose of the present work is to analyze the plastic zone at the front of a mode I crack using the hardness method. With this method, we will determine the shape and dimensions of the plastic zone in some directions and the distribution of stress intensities.

1. Experimental Methods. Flat and compact specimens made of 12Kh18N10T steel were tested. The data needed to determine the dependence of stress intensity on hardness were obtained in testing the flat specimens, while the compact specimens were employed to determine the hardness in the vicinity of the crack front.

S. P. Timoshenko Institute of Mechanics, National Academy of Sciences of Ukraine, 3 Nesterova St., Kyiv, Ukraine 03057, e-mail: fract@inmech.kiev.ua. Translated from Prikladnaya Mekhanika, Vol. 54, No. 2, pp. 106–112, March–April, 2018. Original article submitted August 31, 2016.

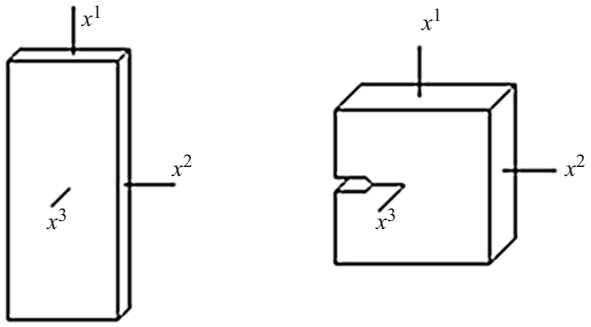

a *b*

Fig. 1

The thicknesses of flat and compact specimens were equal to $3\cdot10^{-3}$ and $10\cdot10^{-3}$ m, respectively. The length of the crack in the compact specimens was equal to $11\cdot10^{-3}$ m. To test the specimens, a TsDMU-30t testing machine with accuracy of loading ±1% was used.

The hardness was determined with a PMT-3 device. Note that the accuracy of hardness measurements depends on the load applied to an indenter. The accuracy increases with the load. The least load on the indenter at which the accuracy can be considered sufficient is equal to 0.049 N. We determined the hardness under a load of 1.961 N which provided high accuracy (±1.5%).

In the testing, we measured both diagonals of each impression, then calculated the arithmetic mean of the results and found the hardness, repeating this operation 10 times. Next we calculated the mean hardness.

Let us now determine the dependence of stress intensity on hardness.

The stress intensity X is described as square root of the second invariant of the stress deviator. The quantity X can be expressed in terms of the first and second invariants of the stress deviator $\boldsymbol{S}$:

$$X = \sqrt{\Lambda - \frac{\Theta^2}{3}}, \tag{1.1}$$

where

$$\Theta = g_{\alpha\beta} S^{\alpha\beta}, \quad \Lambda = g_{\alpha\gamma} g_{\beta\delta} S^{\alpha\beta} S^{\gamma\delta}. \tag{1.2}$$

Here $S^{\varepsilon\zeta}$ are the contravariant components of the tensor $\boldsymbol{S}$.

In the rectangular orthogonal Cartesian coordinate system x^1, x^2, x^3 fixed to the specimens, we have

$$g_{\varepsilon\zeta} = \begin{cases} 1, & \varepsilon = \zeta, \\ 0, & \varepsilon \neq \zeta. \end{cases} \tag{1.3}$$

Note that the axes x^1 and x^2 are aligned with the longitudinal and transverse axes of the specimens (Fig. 1*a*). As is seen, only the component S^{11} is nonzero

$$S^{\varepsilon\zeta} = 0 \quad (\varepsilon = \zeta = 2, 3, \varepsilon \neq \zeta). \tag{1.4}$$

With (1.3) and (1.4), invariants (1.2) are expressed as follows:

$$\Theta = S^{11}, \quad \Lambda = S^{11} S^{11}. \tag{1.5}$$

With (1.5), formula (1.1) becomes:

$$X = \sqrt{2/3}\, S^{11}. \tag{1.6}$$

TABLE 1

$\dot{X}$, Pa	$\dot{H}$, Pa
207.45	1.53334
237.58	1.73673
264.47	1.86717
322.18	2.04885

We used four specimens. After application of the load, we measured (with accuracy up to $\pm 0.5 \cdot 10^{-6}$ m) the transverse dimensions (along the x^2-axis) of the specimens with a MIG-1 indicator. As a result, we obtained the following values of the component S^{11}: $254.08 \cdot 10^6$ Pa, $290.98 \cdot 10^6$ Pa, $323.92 \cdot 10^6$ Pa, $394.59 \cdot 10^6$ Pa. Using these values in (6), we found the value of X. Next, we determined the hardness H for each specimen (over the x^3-plane).

Let

$$\dot{X} = X \cdot 10^{-6}, \quad \dot{H} = H \cdot 10^{-9}. \tag{1.7}$$

The values of $\dot{X}$ and $\dot{H}$ calculated with (1.7) are collected in Table 1.

Let us assume that the function $\dot{X}(\dot{H})$ is described by the following expression [4]:

$$\dot{X} = C_0 \varphi_0(\dot{H}) + C_1 \varphi_1(\dot{H}) + C_2 \varphi_2(\dot{H}) + \ldots + C_n \varphi_n(\dot{H}), \tag{1.8}$$

where $\varphi_0(\dot{H})$, $\varphi_1(\dot{H})$, $\varphi_2(\dot{H})$, …, $\varphi_n(\dot{H})$ are Chebyshev's polynomials.

If $\varphi_0(\dot{H}) = 1$, then

$$\varphi_j(\dot{H}) = b_{j,0}\varphi_0(\dot{H}) + b_{j,1}\varphi_1(\dot{H}) + b_{j,2}\varphi_2(\dot{H}) + \ldots + b_{j,j-1}\varphi_{j-1}(\dot{H}) + \dot{H}^j \ (j = 1, 2, \ldots, n), \tag{1.9}$$

where

$$b_{j,k} = -\frac{\left[\dot{H}^j \varphi_k(\dot{H})\right]}{\left[\varphi_k(\dot{H})\varphi_k(\dot{H})\right]} \quad (k = 0, 1, 2, \ldots, j-1). \tag{1.10}$$

The coefficients C_i are evaluated as follows:

$$\widetilde{C}_i = \frac{\left[\dot{X}\varphi_i(\dot{H})\right]}{\left[\varphi_i(\dot{H})\varphi_i(\dot{H})\right]} \quad (i = 0, 1, 2, \ldots, n). \tag{1.11}$$

As calculations with formulas (1.8)–(1.11) show, function (1.8) can be described with sufficient accuracy by the parabola

$$\dot{X} = 677.40508 - 701.06581\dot{H} + 257.44010\dot{H}^2. \tag{1.12}$$

In what follows, we will consider how the hardness at the crack front is determined. Since plastic deformation results in hardness change, a vicinity of the crack front that is not larger than the plastic zone was subject of interest. In tests of three specimens, the load N applied was equal to 4903.32 N, 5393.65 N, and 5883.99 N, respectively. The crack did not move in the first and second specimens and started in the third specimen.

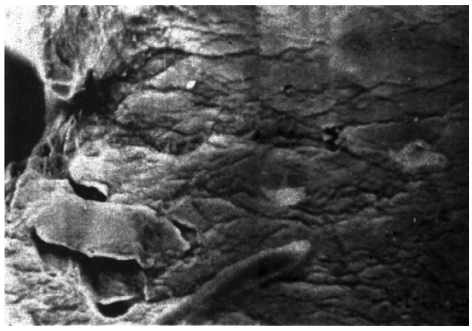

Fig. 2

TABLE 2

$x^1 \cdot 10^3$, m	$x^2 \cdot 10^3$, m					
	0	0.1	0.2	0.3	0.4	0.5
0.2	2.19625	2.05175	1.90731	1.77760	1.70603	1.68312
	379.45	322.73	276.77	244.66	230.65	226.72
0.4	2.23044	2.13021	1.97756	1.85378	1.80246	1.72940
	394.44	352.19	297.78	262.47	250.14	234.94
0.6	2.23044	2.14644	1.97756	1.92106	1.84074	1.78996
	394.44	358.68	297.78	280.69	259.21	249.35
0.8	2.11416	2.02158	1.93495	1.89371	1.81509	1.76536
	345.91	312.24	284.74	273.00	253.05	242.08
1.0	1.99207	1.96320	1.88025	1.84074	1.78996	1.74126
	302.44	293.28	269.36	259.21	247.35	237.22
1.2	1.89371	1.88025	1.85378	1.81509	1.76536	1.71765
	273.00	269.36	262.47	253.05	242.08	232.75
1.4	1.81509	1.81509	1.78996	1.76536	1.74126	1.70603
	253.05	253.05	247.35	242.08	237.22	230.65
1.6	1.76536	1.77760	1.75325	1.74126	1.70603	1.68312
	242.08	244.66	239.60	237.22	230.65	226.72
1.8	1.71765	1.71765	1.72940	1.70603	1.68312	1.66068
	232.75	232.75	234.94	230.65	226.72	223.14

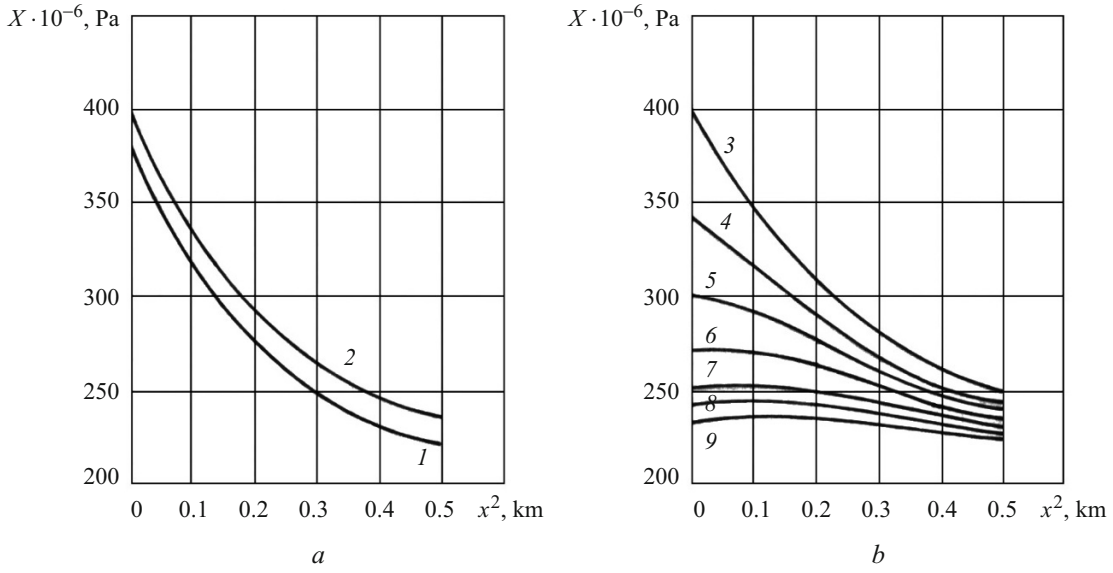

Fig. 3

To describe the specimens, we used a rectangular Cartesian coordinate system x^1, x^2, x^3 with the x^2-axis oriented along the crack, the plane $x^3 = 0$ coinciding with the mid-surface, and the origin being at the crack tip (Fig. 1*b*). The hardness was measured in the planes $x^3 = 0$, $x^3 = 2 \cdot 10^{-3}$ m and $x^3 = 4 \cdot 10^{-3}$ m.

Since the plane $x^3 = 0$ is in the state of plane strain, the results obtained for this plane are the most interesting.

First, we examined, using a BS-301 electron microscope, the surface of the specimens near the crack tip. It was established that before the crack starts, a fracture process zone (destruction zone) with microcracks, pores, and laminations arises ahead of the crack (Fig. 2).

Note that the fracture process zone is usually taken into account in solving boundary-value problems of fracture mechanics [11, 12, 14].

3. Analysis of the Results. Let us analyze the results obtained for the plane $x^3 = 0$ of the third specimen. Using the hardness values and the second formula from (1.7), we determine the values of $\dot{H}$ and then, with (1.12), the values of $\dot{X}$. The values of $\dot{H}$ and $\dot{X}$ are summarized in Table 2 as upper and lower, respectively.

Using the values of $\dot{X}$ and the first formula in (1.7), we determine the values of X, which were used to plots the curves in Fig. 3. The coordinate x^1 corresponding to these plots has the following values: $0.2 \cdot 10^{-3}$ m (curve *1*), $0.4 \cdot 10^{-3}$ m (curve *2*), $0.6 \cdot 10^{-3}$ m (curve *3*), $0.8 \cdot 10^{-3}$ m (curve *4*), $1.0 \cdot 10^{-3}$ m (curve *5*), $1.2 \cdot 10^{-3}$ m (curve *6*), $1.4 \cdot 10^{-3}$ m (curve *7*), $1.6 \cdot 10^{-3}$ m (curve *8*), $1.8 \cdot 10^{-3}$ m (curve *9*).

It should be noted that the stress intensity for $x^1 < 0.2 \cdot 10^{-3}$ m and $x^2 < 0.5 \cdot 10^{-3}$ m is noticeably lower because of the presence of the fracture process zone.

Let us consider how the stress intensity changes with the x^1-coordinate. As the coordinate increases from $0.2 \cdot 10^{-3}$ m to $0.4 \cdot 10^{-3}$ m, the stress intensity increases. As the x^1-coordinate increases from $0.6 \cdot 10^{-3}$ m to $1.8 \cdot 10^{-3}$ m, the stress intensity decreases, which is true for $x^2 < 0.5 \cdot 10^{-3}$ m.

Using the plots in Fig. 3, we determined the coordinates x^1 and x^2 of the points at which the stress intensity takes equal values. These coordinates were used to plot the curves in Fig. 4, where the values of X for curves *1* and *2* are $280 \cdot 10^6$ Pa and $260 \cdot 10^6$ Pa, respectively.

As can be seen, the plastic zone is elongated along the x^1-axis. This fact is in agreement with the numerical solution of the boundary-value problem of the equilibrium of an elastoplastic body with a mode I crack [5].

The dimensions of the plastic zone along the axes x^α ($\alpha = 1, 2$) are denoted by $d^{(\alpha)}$. They were determined as distances from the origin to the points on the axes x^1 and x^2 at which $X = 213.02 \times 10^6$ Pa.

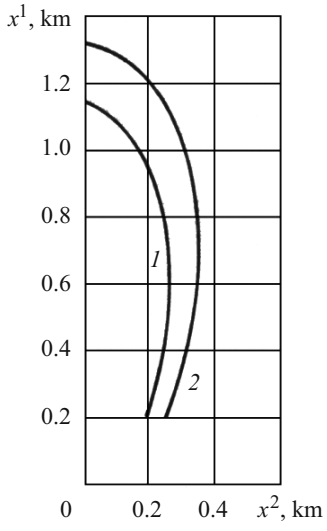

Fig. 4

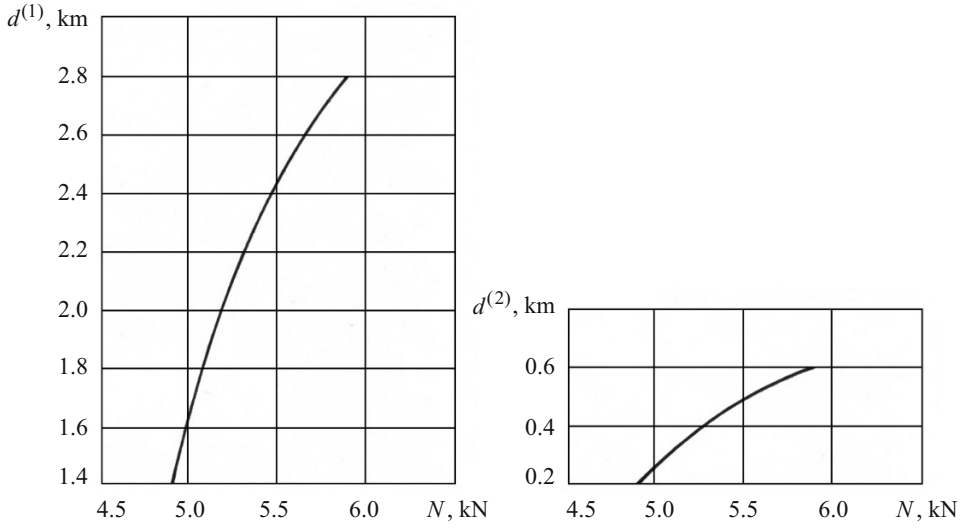

Fig. 5

Figure 5 demonstrates how the dimensions of the plastic zone depend on the load N. The curves are similar. However, the rates at which the dimensions of the plastic zone along the axes x^1 and x^2 increase are essentially different. For example, the rate of increase in the dimension $d^{(1)}$ is much higher than the rate of increase in the dimension $d^{(2)}$. This is natural because the dimension $d^{(1)}$ is much larger than $d^{(2)}$. In the planes $x^3 = 2 \cdot 10^{-3}$ m and $x^3 = 4 \cdot 10^{-3}$ m, the plastic zone is more elongated along the x^2-axis. The dimensions of the plastic zone along the axes x^1 and x^2 increased.

Conclusions. We have studied experimentally the plastic zone at the front of a mode I crack. Using hardness measurements, we have determined the distribution of stress intensities. The fracture process zone near the crack has been discovered. It has been shown how this zone affects the distribution of stress intensity, from which the shape of the plastic zone has been determined. The dimensions of the plastic zone in two mutually orthogonal directions have been determined.

The results obtained can be used to validate crack models and solutions of boundary-value problems of the limit equilibrium of an elastoplastic body with a mode I crack.

REFERENCES

1. G. D. Del', *Determination of Stresses in a Plastic Range from Hardness Distribution* [in Russian], Mashinostroenie, Moscow (1971), p. 200.
2. G. D. Del', L. K. Spiridonov, I. N. Temnik, and K. N. Tsukublina, "On the relation between hardness and stresses in the plastic range," *Mekh. Tverd. Tela*, No. 6, 157–159 (1970).
3. G. D. Del', "Hardness of a deformable body," *Izv. AN USSR: Metally*, No. 4, 97–102 (1967).
4. Yu. V. Linnik, *The Least-Square Method and Fundamentals of the Theory of Observation Processing* [in Russian], Fizmatgiz, Moscow (1958).
5. V. Z. Parton and E. M. Morozov, *Mechanics of Elastoplastic Fracture* [in Russian], Nauka, Moscow (1985).
6. A. M. Rozenberg and L. A. Khvorostukhin, "Hardness and stress in a plastically deformed body," *J. Techn. Fiz.*, **25**, No. 2, 313–322 (1955).
7. P. W. Bridgman, "The compressibility of thirty metals as a function of pressure and temperature," *Proc. Academy of Arts and Sci.*, **58**, No. 5, 166–242 (1923).
8. W. W. Gerberich and J. L. Swedlow, "Plastic strains and energy density in cracked plates," *Exper. Mech.*, **4**, No. 11, 335–344 (1964).

9. G. T. Hahn, R. G. Hoagland, and A. R. Rosenfield, ”Local yielding attending fatigue crack growth,” *Met. Trans.*, No. 3, 1189–1196 (1972).
10. G. T. Hahn, R. G. Hoagland, and A. R. Rosenfield, ”Local yielding and extension of a crack under plane stress,” *Acta Met.*, **13**, No. 3, 293–306 (1965).
11. A. A. Kaminsky and E. E. Kurchakov, ”Influence of tension along a mode I crack in an elastic body on the formation of a nonlinear zone,” *Int. Appl. Mech.*, **51**, No. 2, 130–148 (2015).
12. A. A. Kaminsky and M. F. Selivanov, ”Modeling subcritical crack growth in a viscoelastic body under concentrated forces,” *Int. Appl. Mech.*, **53**, No. 5, 538–544 (2017).
13. D. P. Rooke and F. J. Bradshaw, “A study of crack tip deformation and derivation of fracture energy,” in: *Proc. 2th. Int. Conf. on Fracture*, Chapman and Hall, London (1969), pp. 46–57.
14. M. F. Selivanov, ”Slow growth of a crack with contacting faces in a viscoelastic body,” *Int. Appl. Mech.*, **53**, No. 6, 617–622 (2017).
15. B. J. Shalffer, H. W. Liu, and J. S. Ke, ”Deformation and the strip necking zone in a cracked steel sheet,” *Exper. Mech.*, **11**, No. 4, 286–292 (1971).
16. L. V. Voitovich, M. P. Malezhik, and I. S. Chernyshenko, “Photoelastic modeling of the fracture of viscoelastic orthotropic plates with a crack,” *Int. Appl. Mech.*, **46**, No. 6, 677–682 (2010).